Journal of the European Ceramic Society 20 (2000) 453–462

SiC/Si_3N_4 nano/micro-composite — processing, RT and HT mechanical properties

P. Šajgalík [a,*], M. Hnatko [a], F. Lofaj [b], P. Hvizdoš [b], J. Dusza [b], P. Warbichler [c], F. Hofer [c], R. Riedel [d], E. Lecomte [d], M.J. Hoffmann [e]

[a] *Institute of Inorganic Chemistry, Slovak Academy of Sciences, Dúbravská cesta 9, SK-842 36 Bratislava, Slovakia*
[b] *Institute of Materials Research, Slovak Academy of Sciences, Watsnova 47, SK-043 53 Košice, Slovakia*
[c] *Forschungsinstitut für Elektronenmikroskopie und Feinstrukturforschung, Technische Universität Graz, Steyrergasse 17, A-8010 Graz, Austria*
[d] *FG Disperse Feststoffe, FB Materialwissenschaft, Technische Universität Darmastadt, Petersenstr. 23, D-64287 Darmstatd, Germany*
[e] *Institut für Keramik im Maschinenbau, Universität Karlsruhe, Heid-und-Neu Str. 7, D-76131 Karlsruhe, Germany*

Received 1 April 1999; received in revised form 17 June 1999; accepted 28 June 1999

Abstract

Two SiC/Si_3N_4 nano/micro composites were prepared from a starting mixture of crystalline α-Si_3N_4, amorphous SiNC, Y_2O_3 and/or Al_2O_3. The composite material for room temperature (RT) application has high strength of 1200 MPa, Weibull modulus of 19 and moderate fracture toughness of 7 MPa $m^{1/2}$. The composite for high temperature (HT) application, without Al_2O_3 has RT strength of 710 MPa and is able to keep 60% of its RT strength up to 1300°C. The creep resistance of composite material is approx. 1 order higher compared to relative monolith up to 1400°C.

Keywords: Creep; Mechanical properties; Composites; SiC; Si_3N_4

1. Introduction

SiC/Si_3N_4 nano/micro composites are a new generation of ceramic materials developed a few years ago.[1–3] These composites consist of Si_3N_4 micro-grains and SiC nano-inclusions, which are located within the host Si_3N_4 grains and on their grain boundaries. Enhanced room as well as high temperature properties are reported for nano/micro composites prepared by hot-pressing of CVD SiNC amorphous powder.[1,2] Hot-pressing or gas pressure sintering of a mechanical mixture of sub-micrometer crystalline Si_3N_4 and SiC powders are the other reported ways used for processing of nano/micro composites.[3–5] Composites prepared in such ways have not reached the properties of the CVD derived materials. The present paper introduces a processing method which is a compromise between both above-mentioned approaches; the nano/micro composites were prepared by the addition of polymer derived amorphous SiNC powder into the crystalline Si_3N_4 starting mixture. A similar way of processing was used in Ref. 6 where instead of polymer derived amorphous SiNC, powder plasma spray synthesized powder was used. The room temperature (RT) and high temperature (HT) properties of nano/micro composites prepared by the way presented in the present work are reported and discussed.

2. Experimental

Two basic types of materials were prepared in the framework of the present study: the materials for RT application and material for HT application. The chemical composition of both are listed in Table 1. For each nano/micro composite the reference material was prepared in order to have a possibility to compare the mechanical properties. SiC/Si_3N_4 nano/micro-composites were prepared by seeding of the starting powder with amorphous SiNC fine powder.

The nano/micro composites for this study were prepared by using SiNC amorphous powder prepared by

* Corresponding author.

0955-2219/00/$ - see front matter
PII: S0955-2219(99)00176-4

Table 1
Composition and sintering method used in processing of samples for RT and HT measurements

Properties	Sample	Sintering method	Si_3N_4 wt%	Al_2O_3 wt%	Y_2O_3 wt%	Amorph SiNC wt%
RT	SNYA	GPS 1900°C/2 h	92	3.4	4.6	–
RT	SNYA10	GPS 1900°C/2 h	82	3.4	4.6	10
HT	SNY	HP 1750°C/2 h	95	–	5	–
HT	SNY20	HP 1750°C/2 h	75	–	5	20

pyrolysis of polysilazane based precursor NCP 200 at TU Darmstadt as a micro/nano-structure forming additive. The amorphous SiNC powder, with calculated composition given in Table 2, was added together with the alumina (Alcoa, USA, grade A16) and/or yttria (H.C. Starck, Germany, grade Fine) in the amount listed in Table 1 to the crystalline Si_3N_4 powder (UBE Industries, Ltd., Japan, grade SN-E10), then attrition milled in isopropanol for 4 h.

Dried starting mixtures were sieved through a 25 μm sieve in order to get rid of large agglomerates. The samples for room temperature testing contain alumina as well as yttria. The dried powder mixtures SNYA and SNYA10, respectively (Table 1), were cold isostatically pressed (CIP) at a pressure of 750 MPa in the rubber form. The CIPed samples were gas pressure sintered in a BN crucible at 1900°C for 2 h in a nitrogen atmosphere of 10 MPa. The temperature was measured by a pyrometer Ircon Modline. The density of samples measured by the water immersion method was >99% theoretical density (TD). TD of 3.276×10^3 kg m^{-3} was calculated by the rule of mixtures based on the assumption that, after gas pressure sintering, the added amorphous SiNC powder will crystallize in the amount listed in Table 2.

Samples for high temperature testing, SNY and SNY20, respectively (Table 1) were cold pressed in the steel die with a pressure of 100 MPa, then embedded into the BN and hot-pressed by pressure of 30 MPa at 1750°C and 0.2 bar over-pressure of nitrogen. The density of hot-pressed samples as measured by the mercury immersion method and for all samples was >98% TD. Calculated TD was 3.26×10^3 kg m^{-3}.

A schematic of the processing procedure for both types composites is shown in Fig. 1.

The bars of (45 × 4 × 3) mm for mechanical testing were cut from densified prisms (50 × 15 × 10) mm after gas pressure sintering and discs (50 mm diameter and 5 mm height) after hot pressing, respectively. The bars with tensile surface polished to 15 μm finish were used for the four-point bending tests (20/40 inner/outer span, cross-head speed 0.5 mm/min) at room temperature. Fracture toughness was measured by the indentation method and calculated using the formula of Shetty.[7]

High temperature bending strength was measured on air in four-point bending mode (20/40 inner/outer span, cross-head speed 0.3 mm/min) at temperatures listed in Table 5. The creep tests in bending (20/40 inner/outer span) were performed in air from 1200 to 1400°C, with step 50°C. The stepwise loading regime was selected at each temperature. The creep experiment started with a load of 50 MPa for 24 h, then 100 MPa for the next 24 h and 150 MPa for the last 24 h in order to speed up the accquiring of data.

The microstructure and the grain boundaries were investigated by TEM. Analytical transmission electron microscopy was performed using a Gatan imaging filter mounted on a Philips CM20/Stem (acceleration voltage 200 keV; equipped with LaB6 cathode). By dimpling of Si/N/C composite of thickness 100 μm a thickness of about 20 μm was achieved; the thin foil was then ion-milled until perforation.[8,9]

Table 2
Calculated proposition proposed to originate during sintering of ceramic composite after crystallization of the amorphous Si–N–C powder

Si_3N_4 wt%	SiC wt%	Free carbon wt%
66.36	27.21	6.43

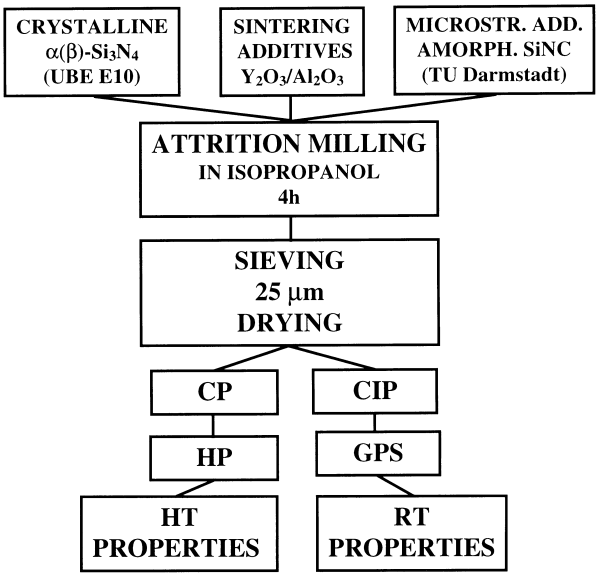

Fig. 1. Processing procedure of nano/micro composites used in the present paper.

The XRD was used for assessment of effect of SiC inclusions on the major Si_3N_4 phase. A Stoe diffractometer (Darmstadt, Germany) was used for XRD measurements. The diffraction pattern was taken in reflection mode from the surface of SNY and SNY20 samples polished together in one epoxy body to 1 μm finish for 10 h. The long time of polishing was used for minimizing the surface residual stresses, one epoxy body for both samples was used in order to avoid different treatment of both samples.

3. Results

3.1. Microstructure

3.1.1. Composite SNYA10

SNYA10 nano/micro composite with density of 3.247 $\times 10^3$ kg m^{-3} was prepared by seeding the starting mixture with a fine amorphous SiNC powder by gas pressure sintering.

The TEM-bright field image in Fig. 2 shows the typical microstructure which is homogeneous without any observable macro-defects. The microstructure consists of elongated grains with the mean diameter below 1 μm and with lengths up to 10 μm. An elemental map showed that the composite microstructure besides Si_3N_4 micro-grains contains smaller SiC grains of size 300–600 nm. A detailed

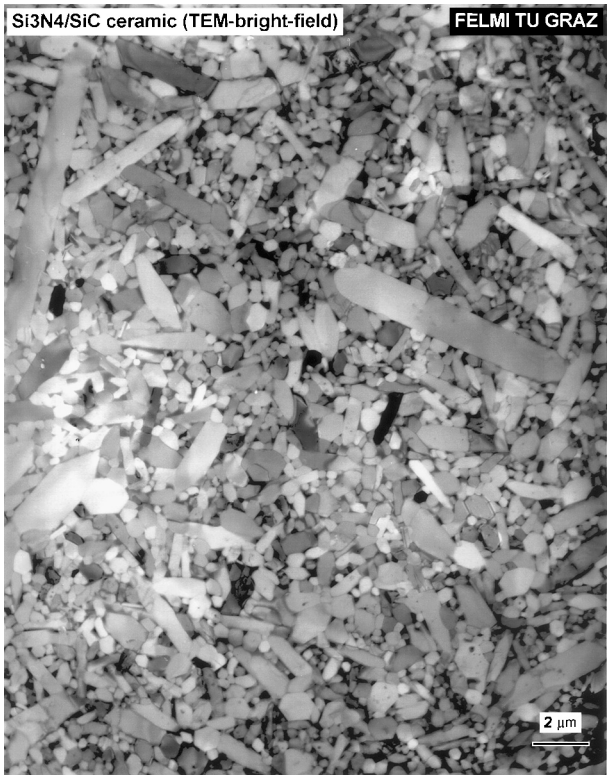

Fig. 2. The TEM-bright field image of SNYA10 nano/micro-composite. Bar 2 μm.

TEM investigation at higher magnification revealed that the majority of Si_3N_4 grains contain randomly distributed SiC nano-inclusions of size from 5 to 100 nm, (Fig. 3).

The elemental maps of Si, N, C and O taken from such a Si_3N_4 grain confirm the SiC composition of the nano-inclusion with a thin oxygen rich surface layer, [Fig. 3(b)-(e)].

An elemental map of another Si_3N_4 grain of the same SNYA10 composite is shown in Fig. 4. The SiC nano-inclusions of this Si_3N_4 grain are oxygen free as can be seen in Fig. 4(d). A bright field TEM image of such a SiC nano-inclusion contains the strain contrast (foil bend contour) joining the SiC inclusion and grain boundary, [Fig. 4(a)]. No chemical inhomogeneity along this line was observed [Fig. 4(b)–(d)].

TEM investigations showed that the SNYA10 nano/micro composite consists of four different grains. These can be classified as follows: Si_3N_4 micro-grains, SiC sub-micro-grains, and two types of Si_3N_4 micro-grains with SiC nano-inclusions. These are Si_3N_4 micro-grains containing oxygen free SiC nano-inclusions and SiC nano-inclusions with oxygen rich surface layer, respectively [Figs. 3(e) and 4(d)]. No other grains or areas with different chemical compositions, e.g. free carbon, were found.

3.1.2. Composite SNY20

Similar, but finer, microstructure was observed also for the composite SNY20. The distribution of the SiC grains taken from TEM micrographs of sample SNY20 is shown in Fig. 5. The larger grains were found at the grain boundaries (inter SiC grains), the finer SiC were determined within the Si_3N_4 host grains (intra SiC grains). Two frequency maximum of intra SiC nanograins were found with size approx. 25 and 75 nm, respectively, while the inter SiC grains have the frequency maximum at 225 nm (Fig. 5). The number of intra vs inter SiC grains was estimated from TEM micrographs, the ratio is 80 vs 20 for SNY20 nano/micro composite.

The presence of SiC grains introduced residual stress into the composites. XRD patterns taken from the polished surface of both SNY and SNY20 samples show the shift of silicon nitride 101 and 200 reflections of sample SNY20. This shift towards smaller angles means the decrease of unit cell dimension of silicon nitride phase in SNY20 composite. Silicon nitride unit cell dimensions of SNY and SNY20 calculated from XRD pattern are listed in Table 3.

3.2. Mechanical properties

3.2.1. RT properties

3.2.1.1. Fracture toughness. The fracture toughness of both ceramic materials were measured by indentation method and these are listed in Table 4. The fracture toughness of SNYA (7.4 MPa m$^{1/2}$) is slightly higher

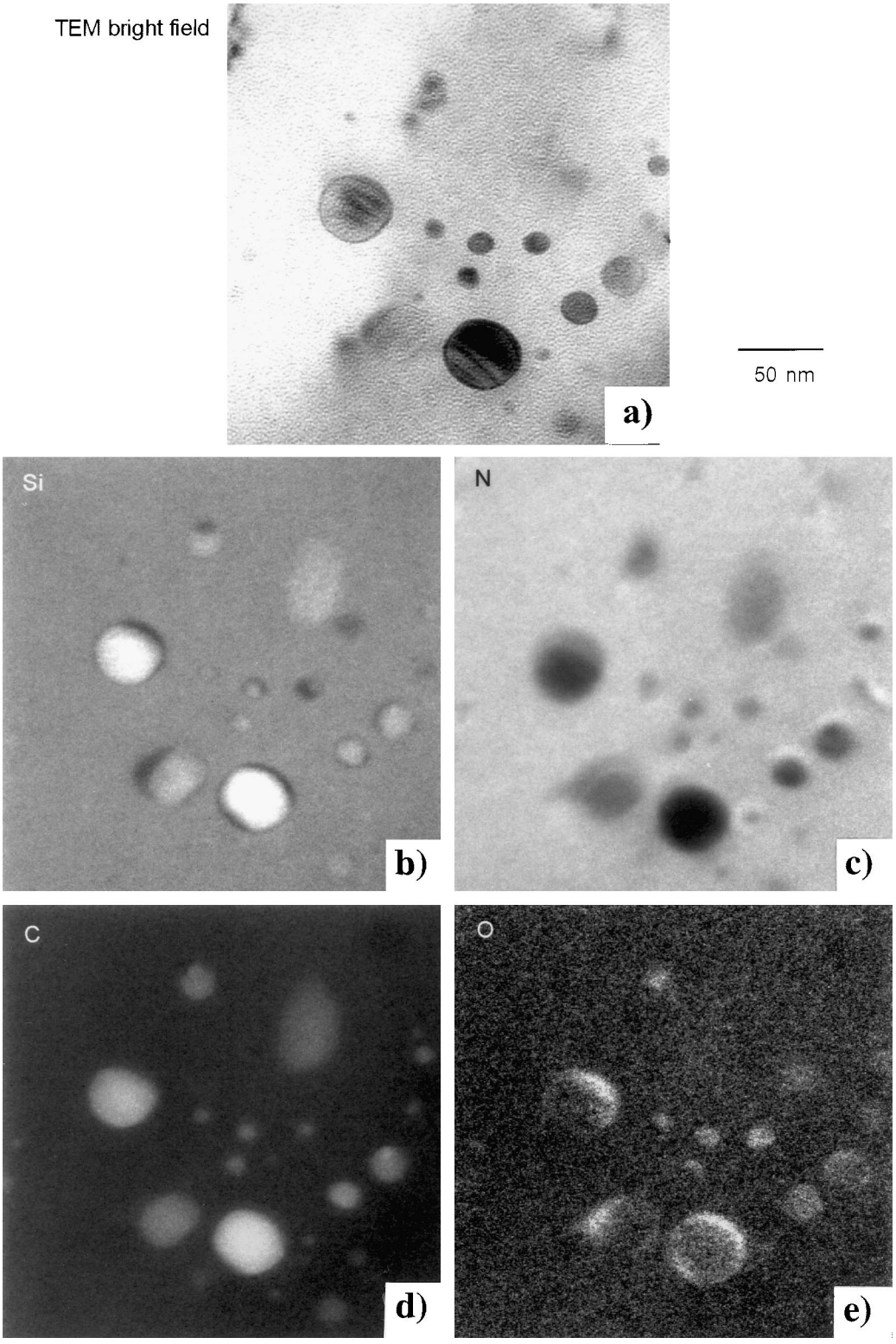

Fig. 3. (a) The TEM-bright field image of SiC nano-inclusions within the Si_3N_4 micro-grain. Bar 50 nm. (b) Si; (c) N; (d) C; and (e) O elemental map of the same area.

compared to SNYA10 (6.9 MPa $m^{1/2}$). A higher difference in fracture toughness was observed for SNY and SNY20 ceramics, 7.1 and 6.4 MPa $m^{1/2}$, respectively. The slightly decreased fracture toughness of both nano/micro composites compared to the relative monolithic materials is attributed to a low number of intra SiC grains, only 20% (see previous paragraph). As was documented recently,[10] the intra inclusions of the second

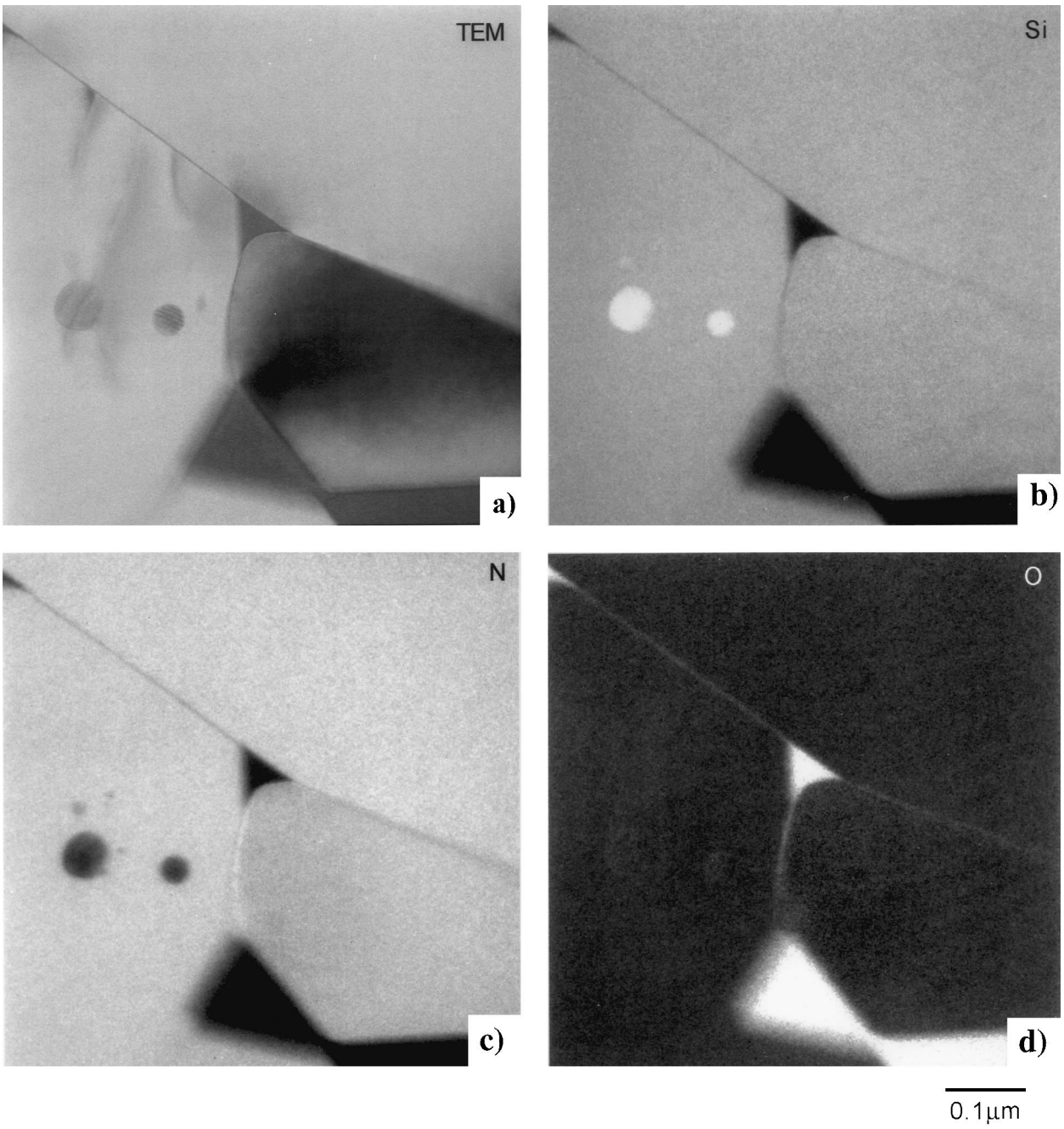

Fig. 4. (a) The TEM-bright field image of SiC nano-inclusions within the Si_3N_4 micro-grain. Bar 0.1 μm. (b) Si; (c) N; and (d) O elemental map of the same area.

phase with similar ratio of thermal expansion coefficients as in present case, have a positive effect on the fracture toughness of two phase composite. The role of the residual stresses cannot be neglected in the present case. These are discussed in more detail later.

3.2.1.2. Bending strength and Weibull modulus. The bending strength of both ceramic materials is relatively high. Room temperature materials have the higher values, 990 MPa for SNYA and 1200 MPa for SNYA10, respectively; the strength of high temperature materials is lower, 870 MPa for SNY and 710 MPa for SNY20, respectively, Table 4. The high strength of SNYA nano/micro composite is attributed to its higher microstructural homogeneity. No abnormal large grains were observed in this composite. No macrodefects as fracture origins were identified on the fracture surface. This observation corresponds with the relatively high Weibull modulus of almost 20 for SNYA10 compared to the 7 for SNYA (Table 4).

3.2.2. HT properties

These were exclusively studied for the materials SNY and SNY20, respectively.

3.2.2.1. HT bending strength. The bending strength at different temperatures of nano/micro composite (SNY20) and reference monolithic material (SNY) are listed in Table 5.

The bending strength of composite SNY20 measured at elevated temperatures is higher compared to the strength of monolithic SNY, while at room temperature it is vice versa. Composite SNY20 keeps 60% of room temperature strength up to 1300°C, while the monolithic only 40%, moreover the strength of the composite is almost constant in the measured temperature interval from 1000 to 1300°C. This increase of HT bending strength of SNY20 composite is attributed to the change of grain boundary phase. The model experiment simulating the formation of the grain boundary phase of SNY20 nano/micro composite is described in the discussion.

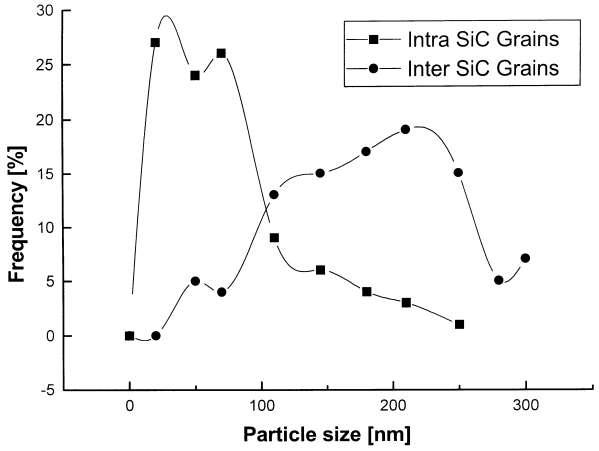

Fig. 5. SiC grains distribution within the sample SNY20.

Table 3
Si_3N_4 unit cell dimensions calculated from XRD patterns

Unit cell dimension	SNY	SNY20
a (A)	7.602845 ± 0.000613	7.598296 ± 0.000666
c (A)	2.907161 ± 0.000403	2.906002 ± 0.000409
Volume (A^3)	145.53	145.30

Table 4
RT mechanical properties

Sample	Fracture toughness (MPa $m^{1/2}$)	Bending strength (MPa)	Weibull modulus
SNYA	7.4	990	7
SNYA10	6.9	1203	19
SNY	7.1	870	–
SNY20	6.4	710	–

3.2.2.2. Creep resistance. The creep resistance of reference ceramics, SNY as well as nano/micro-composite, SNY20, in four-point bending was measured in the temperature range of 1200–1400°C at the stresses of 50, 100 and 150 MPa. The strain–time dependencies of SNY and nano/micro composite SNY20, respectively are shown in Fig. 6. This graph shows that nano/micro composite SNY20 is able to withstand the stress of 200 MPa at 1350°C while the related monolithic material SNY was broken at 100 MPa at the same temperature. As can be seen from this figure the duration of the beginning of steady state creep in both materials is quite similar. The different slopes of both step-curves indicate the difference of strain rates of both composites. Fig. 7 shows that nano/micro composite SNY20 has higher creep resistance compared to the reference material 5SNY. Strain (creep) rate is almost 1 order of magnitude lower for SNY20 nano/micro composite compared to the reference SNY material. The difference is smaller at higher temperatures. The apparent activation energy of SNY20 at stress load 100 MPa is 566 kJ/mol, for reference material SNY this value is only 289 kJ/mol. The slopes of strain–stress dependencies of SNY are from the range $2 > n > 1$ (Fig. 8), which indicates that the proposed creep mechanisms is weakening of the glassy grain boundary phase.[11] For the nano/micro composite the exponents are almost 1 [with the exception of creep at 1200°C when the $n = 0.7$ and 1350°C when the $n = 1.4$, (Fig. 9)]. This indicates diffusion creep. The change of a creep mode from weakening of grain boundary phase to diffusion creep is partially proved also by TEM observations. While in the sample SNY a frequent cavitation after creep test was observed, (Fig. 10), the sample SNY20 was almost free of cavities.

Table 5
Bending strength of nano/micro composite and relative monolithic material

	Temperature (°C)				
	RT	800	1000	1200	1300
Strength of SNY (MPa)	870	400	421	360	325
Ratio to the RT strength		0.46	0.48	0.41	0.37
Strength of SNY20 (MPa)	710	Not measured	440	440	415
Ratio to the RT strength		Not measured	0.62	0.62	0.58

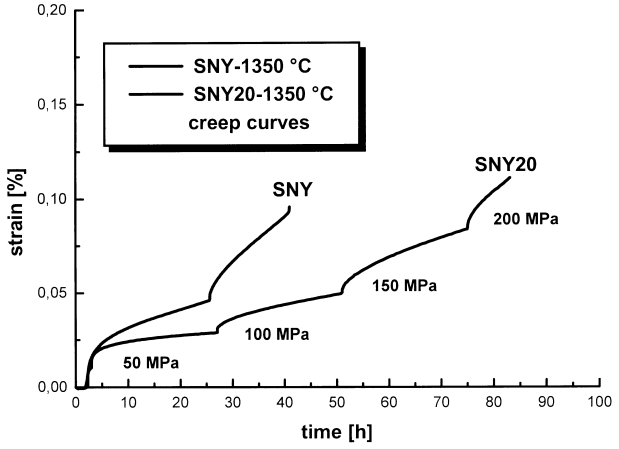

Fig. 6. Creep deformation at 1350°C of SNY and SNY20 at various loads.

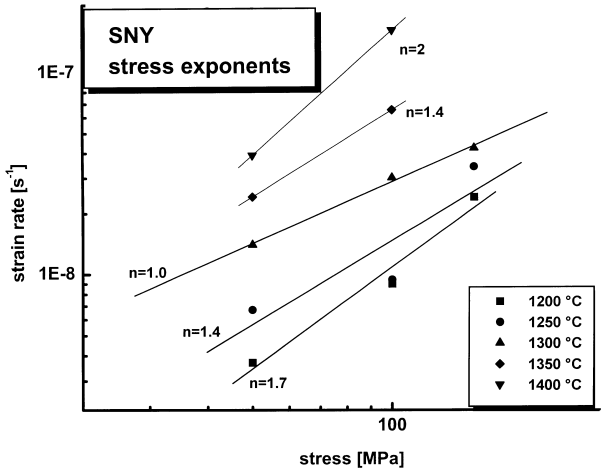

Fig. 8. Strain rate–stress dependence of SNY at various temperatures.

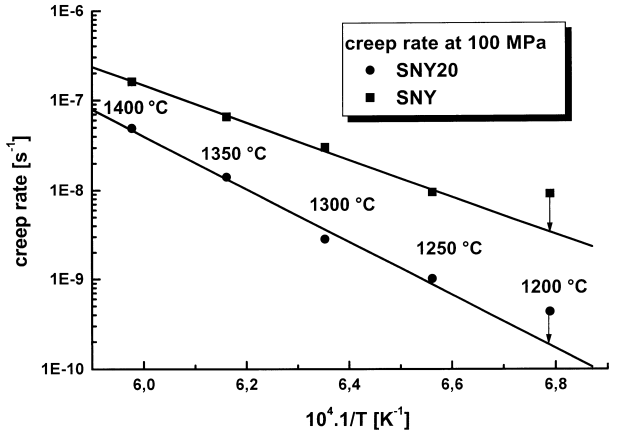

Fig. 7. Comparison of creep rates for 5SNY and 5SNY20, respectively. The arrows indicate the measurements in which the steady state creep was probably not reached.

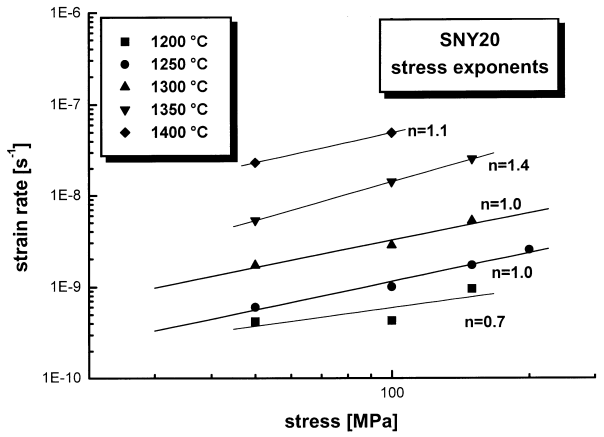

Fig. 9. Strain rate–stress dependence of SNY20 at various temperatures.

4. Discussion

4.1. Room temperature properties

SNYA10 nano/micro composite prepared in the present study has higher strength and Weibull modulus compared to the reference SNYA material. The increased strength of nano/micro composite SNYA (almost 20% to the value of 1.2 GPa) is in contradiction to the recently published extensive work of Herrmann et al. on SiC/Si_3N_4 nano-composites[4]. Herramnn et al.[4] report no effect of the SiC nano-grains on the strength of SiC/Si_3N_4 nano/micro composite. But the presents result fits quite well with the results published by Niihara[1].

No substantial decrease of fracture toughness of nano/micro SNYA10 composite compared to the reference SNY ceramics means that the critical flaw size of SNYA10 is lower ($a = 33\mu m$) than that of SNYA, which is $a = 57\mu mm$. The distinct higher Weibull modulus of SNYA10 confirm the homogeneity of this microstructure, which is also documented by the TEM micrograph shown in Fig. 2. The homogeneity of SNYA10 microstructure is reached by the pinning effect of randomly distributed SiC nano-grains which hinder the abnormal grain growth of Si_3N_4. No β-Si_3N_4 grains with the size >15 μm were observed in the microstructure. This effect was already presented elsewhere.[12,13] Introduction of the SiC nano-grains changes also the stress state of the microstructure. A simple calculation taking into account the difference in thermal expansion coefficient between SiC nano-inclusion and Si_3N_4 host micro-grain and using Hook's law shows that the radial tensile stress of 1.3 GPa is produced around the SiC inclusion by cooling the sample from the sintering temperature to RT when the inclusion is incorporated into the host grain by grain growth mechanisms. This stress is large enough to deform the host Si_3N_4 lattice. Table 3 documents this fact. The

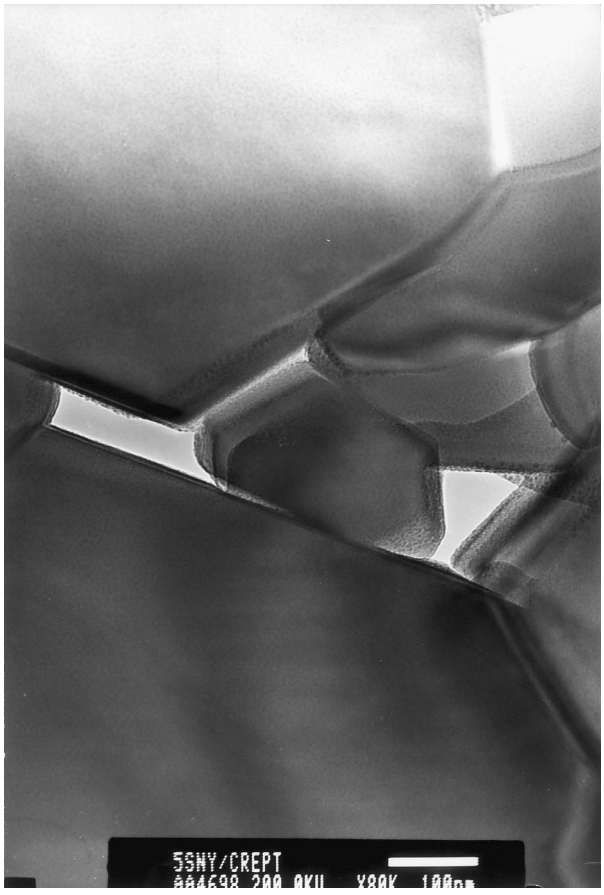

Fig. 10. Cavity formation in sample SNY after creep test.

decrease in lattice parameter of Si_3N_4 host grain in case of nano-composite SNY20 indicates general compressive residual stresses within the composite matrix because of the presence of SiC inclusions. This statement is, at first view, in contradiction with the previous statement. The XRD gives overall information while the simplified Hook's law calculation gives only the radial stresses arising from higher shrinkage of SiC inclusion within the Si_3N_4 host grain. This calculation does not consider a hoop compressive stress arising around the SiC inclusion. This probably, in general exceeds the tensile radial stress and causes the slight compression of the unit cell. The bend contour presented in Fig. 4 clearly documents the stress arising from the presence of SiC nano-inclusion with a "clean" interface, i.e. without any surface oxygen layer.

As was documented for layered composites, [14,15] the residual stresses dramatically influence the mechanical behaviour of each composite. The role of residual stresses with respect to the mechanical properties of presented nano/micro composites is not clear yet, but their importance with respect to the mechanical properties is already accepted and they are presently studied by means of XRD and HRTEM. Besides the role of intra SiC inclusions, these studies also take into account the inter SiC inclusions and the stress status of glassy grain boundary phase.

The amount of SiC phase within the microstructure also plays an important role because of its influence on the grain growth and simultaneously on residual internal stresses. In the work of Sasaki[3] it was pointed out that the optimum amount of SiC nano-grains for room temperature properties is in the range of 5–10 wt%. Using the data from Table 2, the amount of SiC nano-grains present in the SNYA10 nano/micro composite is only 2.7 wt%, i.e. much lower than indicated optimum. Excellent RT properties at such a low amount of SiC phase in general indicate the potential of the presented composite in the sense of possible increase of the fraction of SiC.

4.2. High temperature properties

4.2.1. Creep

The high temperature creep measurements show an improvement of creep resistance of the nano/micro SNY20 composite compared to the reference SNY. The improvement of the creep resistance is usually attributed to the distribution of the fine SiC nano-grains along the grain boundaries.[16] The recent publication of Rendtel et al.[5] shows that there exists an optimum of SiC nano-grains content which lies within the range of 10–15 wt%. The amorphous SiNC powder added in the amount of 20 wt% to the starting mixture yields 5.5 wt% of SiC present in the SNY20 nano/micro composite. This value is far below the 10–15 wt% optimum. In spite of this fact the creep strain of SNY20 is approx. 1 order of magnitude lower compared to the reference SNY ceramics (Fig. 7). On the other hand, a higher addition of amorphous SiNC powder to the starting composition also has limits. The reason for this is an excess of the carbon in the SiCN powder (Table 2).

By deliberately increasing the amount of SiC nano-grains in the microstructure (i.e. increase of SiNC content in the starting composition), the content of a free carbon will also arise. A former study,[13] showed that the effect of excessive carbon on the mechanical properties was strongly negative. As was shown in this paper, the nano/micro composite with a 3 wt% excess of free carbon contained the non-reacted carbon regions of several micrometers after hot pressing, which served as the fracture origins. In the present work, as was mentioned before, no carbon regions within the microstructure of either of SNYA10 or SNY20 were observed by SEM and TEM.

4.2.2. Role of free carbon

For the assessment of the carbon role, model experiments were performed. Y_2O_3 and SiO_2 in the eutectic composition according to the phase diagram (eutectic temperature 1660°C) [17] with the addition of 1 and 5 wt% C were heated at 1750°C for 2 h in a nitrogen atmosphere. Neither composition was melted after

the heating cycle. XRD analysis of cooled and ground samples showed the presence of both $Y_2Si_2O_7$ and Y_2SiO_5 crystalline phases. No carbon was visually detected after heating cycles, and the samples were completely white. The DTA analysis of grounded model samples showed no weight loss on heating in air up to 1000°C, i.e. no oxidation of non-reacted carbon was present. According to the binary Y_2O_3–SiO_2 phase diagram, at 1750°C with decreasing SiO_2 content, the region of stability move from eutectic melt (1660°C) towards stability of $Y_2Si_2O_7$ and Y_2SiO_5 crystalline phases. In the present case the decrease content of SiO_2 is caused by its reduction with carbon. The reaction:

$$SiO_2 + C = SiO + CO$$

took place. By reduction of SiO_2 the region of dominance of either $Y_2Si_2O_7$ or Y_2SiO_5 phases was changed consequently according to binary Y_2O_3–SiO_2 phase diagram. The reaction product SiO reacted with a nitrogen atmosphere, which was documented by decrease of nitrogen over-pressure in the furnace. The XRD analysis of whiskers taken from the sample surface confirmed the presence of α-Si_3N_4.

The model experiment described above can be used for explanation of creep behaviour of a nano-micro SNY20 composite. The excessive carbon introduced along with SiNC amorphous powder most probably reduced the SiO_2 content similarly as observed in the model experiment. This fact has two consequences:

- decrease amount of oxide grain boundary phase,
- shift of to higher eutectic temperature; according to the phase diagram the next eutectic point (at decreased content of SiO_2) is at 1900°C.

That means the contribution to 1 order increase of creep resistance of nano-micro SNY20 composite compared to the monolithic SNY is not caused only by distribution of SiC submicrometer grains at the grain boundary but by changing the chemistry of grain boundary phase. This explains the rapid increase of creep resistance in the present case; even the content of SiC nano-grains is rather low, 5.5 wt% compared to the optimum of 10–15 wt% suggested by other authors.[5]

The chemistry of the glassy phase in the present case can be also influenced by the solubility of carbon in the oxynitride grain boundary phase, similar to the silicon oxycarbide glasses which have excellent high temperature creep resistance,[18,19] but the model experiments did not confirm their formation.

5. Conclusions

The present study shows that it is possible to prepare SiC/Si_3N_4 micro/nano composite from the powder mixture of amorphous SiNC and crystalline α-Si_3N_4 with oxide sintering additives. Micro/nano composite consists of Si_3N_4 micro-grains and SiC grains of the size from several tens of nanometers to several micrometers. The finer intra SiC grains are located within the host Si_3N_4 grains. For the nano/micro composite SNY20 the ratio of intra vs inter SiC grains is 80:20. The RT bending strength and Weibull modulus of SNYA10 micro/nano composite is high, 1.2 GPa and approx. 20, respectively. The high mechanical properties of this composite are attributed to the microstructure homogeneity caused by the pinning effect of SiC submicrometer grains. The HT bending strength of SNY20 micro/nano composite keeps 60% of the RT strength up to 1300°C. Creep resistance of SNY20 is high, approx. 1 order of magnitude higher compared to the reference SNY material within the temperature interval from 1200 to 1400°C. The increased creep resistance is mainly caused by the change of grain boundary chemistry as a result of carbothermal reduction of silica. The change of creep mechanisms was documented by change of creep exponent from 2 to 1.

Acknowledgements

Present work was partly supported by Slovak Grant Agency VEGA, project 2/5118/99 and Slovak–Germany R&D Program, project X292.11. P. Šajgalík acknowledges also the Alexander von Humboldt Foundation for financial support during his stay at the University of Karlsruhe where a part of the mechanical properties were measured. P. Hvizdoš acknowledges the financial support of the British Council Academic Link "Silicon Nitride for High Temperature Structural Applications". The authors acknowledge Dr. J. Kečkéš for residual stresses measurements. R. Riedel and E. Lecomte acknowledges the financial support of the European Community.

References

1. Niihara, K., New design concept of structural ceramics — ceramic nanocomposites. *J. Jpn. Cer. Soc*, 1991, **99**(10), 974–982.
2. Niihara, K., Suganuma, K., Nakahira, A. and Izaki, K., Interfaces in Si_3N_4 nano-composites. *J. Mater. Sci. Lett*, 1990, **9**, 598–599.
3. Sasaki, G., Suganuma, K., Fujita, T., Hiraga, K. and Niihara, K., Interface structure of Si_3N_4 matrix composite with nanometer scale SiC particles. *Mar. Res. Symp. Proc.*, 1993, **287**, 335–340.
4. Herrmann, M., Schubert, C., Rendtel, A. and Hübner, H., Silicon nitride/silicon carbide nanocomposite materials: I, fabrication and mechanical properties at room temperature. *J. Am. Ceram. Soc.*, 1998, **81**(5), 1094–1108.
5. Rendtel, A., Hübner, H., Herrmann, M. and Schubert, C., Silicon nitride/silicon carbide nanocomposite materials: II, hot strength, creep, and oxidation resistance. *J. Am. Ceram. Soc.*, 1998, **81**(5), 1109–1120.

6. Rendtel, P., Rendtel, A., Hübner, H., Klemm, H. and Herrmann, M., Effect of long term oxidation on creep and failure of Si_3N_4 and Si_3N_4/SiC nanocomposites. *J. Eur. Ceram. Soc.*, 1999, **19**(2), 217–226.
7. Shetty, D. K., Wright, I. G., Mincer, P. M. and Clauer, A. H., Indentation fracture of WC-Co cermets. *J. Mater. Sci.*, 1985, **20**, 1873–1882.
8. Hofer, F., Warbichler, P. and Grogger, W., Nano-Analyse im Elektronenmikroskop. *Spectrum der Wissenschaft*, 1998, **10**, 48–54.
9. Hofer, F. and Warbichler, P., Improved Imaging of secondary phases in solids by energy-filtering TEM. *Ultramicroscopy*, 1996, **63**, 21–25.
10. Nandy, M-O., Schmauder, S., Kim, B-N., Watanabe, M. and Kishi, T., Simulation of crack propagation in alumina particle-dispersed SiC composites. *J. Eur. Ceram. Soc.*, 1999, **19**, 329–334.
11. Cannon, W. R. and Langdon, T. G., Review: creep of ceramics, Part 1 mechanical characteristics. *J. Mater. Sci.*, 1983, **18**, 1–50.
12. Šajgalík, P. and Galusek, D., α/b phase transformation of silicon nitride: homogeneous and heterogeneous nucleation. *J. Mater. Sci. Lett.*, 1993, **12**, 1937–1939.
13. Šajgalík, P., Dusza, J., Hofer, F., Warbichler, P., Reece, M., Boden, G. and Kozánková, J., Structural development and properties of SiC-Si_3N_4 nano/micro composites. *J. Mater. Sci. Lett.*, 1993, **15**, 72–76.
14. Šajgalík, P., Lenčéš, Z. and Dusza, J., Layered Si_3N_4 composites with enhanced room temperature properties. *J. Mater. Sci.*, 1996, **31**, 4837–4842.
15. Šajgalík, P. and Lenčéš, Z., Silicon nitride layered composites — relationship between residual stresses and fracture behavior. In *Ceramics Materials and Components for Engines,* ed. K. Niihara et al. Technoplaza Co., Ltd. 1998, pp. 675–678.
16. Niihara, K., Hirano, T., Izaki, K. and Wakai, F., High temperature creep/deformation of Si_3N_4/SiC nanocomposites. In *Silicon-Based Structural Ceramics*, ed. B.W. Sheldon and S. C. Danforth. Ceramic Transactions, Vol. 42. The American Ceramic Society, OH, 1994, pp. 208–219.
17. Levin, E. M., Robbins, C. R. and McMurdie, H. F., Fig. 2388. In *Phase Diagrams for Ceramists*, ed. M.K. Reser. American Ceramic Society, Columbus, OH, 1969.
18. Soraru, G. D., D'Andrea, G., Campostrini, R., Babonneau, F. and Mariotto, G., Structural characterisation and high-temperature behavior of silicon oxycarbide glasses from sol–gel precursors containing Si–H bonds. *J. Am. Ceram. Soc.*, 1995, **78**(2), 379–387.
19. Soraru, G. D., Dallapiccola, E. and D'Andrea, G., Mechanical characterisation of sol-gel derived silicon oxycarbide glasses. *J. Am. Ceram. Soc.*, 1995, **79**(8), 2074–2080.